AMERICAN SOCIETY FOR MICROBIOLOGY | Journal of Virology®

VACCINES AND ANTIVIRAL AGENTS

Epistastic Interactions within the Junín Virus Envelope Glycoprotein Complex Provide an Evolutionary Barrier to Reversion in the Live-Attenuated Candid#1 Vaccine

Joanne York,[a] Jack H. Nunberg[a]

[a]Montana Biotechnology Center, University of Montana, Missoula, Montana, USA

ABSTRACT The Candid#1 strain of Junín virus was developed using a conventional attenuation strategy of serial passage in nonhost animals and cultured cells. The live-attenuated Candid#1 vaccine is used in Argentina to protect at-risk individuals against Argentine hemorrhagic fever, but it has not been licensed in the United States. Recent studies have revealed that Candid#1 attenuation is entirely dependent on a phenylalanine-to-isoleucine substitution at position 427 in the fusion subunit (GP2) of the viral envelope glycoprotein complex (GPC), thereby raising concerns regarding the potential for reversion to virulence. In this study, we report the identification and characterization of an intragenic epistatic interaction between the attenuating F427I mutation in GP2 and a lysine-to-serine mutation at position 33 in the stable signal peptide (SSP) subunit of GPC, and we demonstrate the utility of this interaction in creating an evolutionary barrier against reversion to the pathogenic genotype. In the presence of the wild-type F427 residue, the K33S mutation abrogates the ability of ectopically expressed GPC to mediate membrane fusion at endosomal pH. This defect is rescued by the attenuating F427I mutation. We show that the recombinant Candid#1 (rCan) virus bearing K33S GPC is viable and retains its attenuated genotype under cell culture conditions that readily select for reversion in the parental rCan virus. If back-mutation to F427 offers an accessible pathway to increase fitness in rCan, reversion in K33S-GPC rCan is likely to be lethal. The epistatic interaction between K33S and F427I thus may minimize the likelihood of reversion and enhance safety in a second-generation Candid#1 vaccine.

IMPORTANCE The live-attenuated Candid#1 vaccine strain of Junín virus is used to protect against Argentine hemorrhagic fever. Recent findings that a single missense mutation in the viral envelope glycoprotein complex (GPC) is responsible for attenuation raise the prospect of facile reversion to pathogenicity. Here, we characterize a genetic interaction between GPC subunits that evolutionarily forces retention of the attenuating mutation. By incorporating this secondary mutation into Candid#1 GPC, we hope to minimize the likelihood of reversion and enhance safety in a second-generation Candid#1 vaccine. A similar approach may guide the design of live-attenuated vaccines against Lassa and other arenaviral hemorrhagic fevers.

KEYWORDS Candid#1, Junín, arenavirus, attenuation, envelope glycoprotein, epistasis, evolution, vaccines, virus entry, membrane fusion

Arenaviruses (genus *Mammarenavirus*) comprise a diverse family of enveloped negative-strand RNA viruses that are endemic to rodent populations worldwide. Some species can be transmitted to humans to cause severe life-threatening hemorrhagic fevers (1, 2). Lassa virus (LASV) is prevalent in western Africa (3), and at least five arenavirus species are known to cause fatal disease in the Americas, including the Argentine hemorrhagic fever virus Junín (JUNV) (1, 4). Without licensed vaccines or

Received 22 September 2017 **Accepted** 16 October 2017

Accepted manuscript posted online 25 October 2017

Citation York J, Nunberg JH. 2018. Epistastic interactions within the Junín virus envelope glycoprotein complex provide an evolutionary barrier to reversion in the live-attenuated Candid#1 vaccine. J Virol 92:e01682-17. https://doi.org/10.1128/JVI.01682-17.

Editor Terence S. Dermody, University of Pittsburgh School of Medicine

Address correspondence to Jack H. Nunberg, jack.nunberg@umontana.edu.

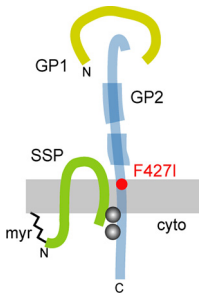

FIG 1 Arenavirus GPC. Schematic drawing of GPC subunit organization. Features include SSP myristoylation (myr), the binuclear SSP-GP2 zinc finger (gray balls), and the N- and C-terminal heptad-repeat regions in GP2 (thick blue), diagnostic of class I viral fusion proteins. The attenuating F427I mutation in Candid#1 is shown in red. The schematic drawing is not to scale, and the relative positions of the subunits are unknown.

specific therapies, hemorrhagic fever arenaviruses pose significant threats to public health and national security. Accordingly, these viruses are recognized as category A priority pathogens by the U.S. Department of Health and Human Services (https://www.niaid.nih.gov/research/emerging-infectious-diseases-pathogens) and as a priority target for vaccine development by the Coalition for Epidemic Preparedness Innovations (http://cepi.net/resources#Priority-diseases).

Epidemic outbreaks of Argentine hemorrhagic fever in agricultural regions near Buenos Aires during the period of 1960 to 1980 highlighted the urgent need for vaccine protection against JUNV infection (5). Collaborative efforts by the Argentine government, the U.S. National Institutes of Health, and the U.S. Army Medical Research Institute for Infectious Diseases culminated in development of the live-attenuated candidate 1 (Candid#1) JUNV vaccine (5). The Candid#1 virus was attenuated in mice, guinea pigs, and rhesus macaques and conferred protection against lethal JUNV infection (6). Under the auspices of a U.S. Investigational New Drug Application, the vaccine was proved to be safe and efficacious in human volunteers (7). Virus-neutralizing antibodies were shown to be responsible for vaccine-mediated protection (8, 9). The Candid#1 vaccine became available in Argentina in 1992 for seasonal use in at-risk populations and has been administered to more than 250,000 persons (10). This vaccine has not been licensed in the United States.

The Candid#1 strain was derived using a classical attenuation strategy of serial passage in guinea pigs, mouse brains, and finally in fetal rhesus lung epithelium cell culture (FRhL-2) (5). During this time, the virus acquired a number of mutations throughout the genome (11–13). Recent reverse genetics studies have identified a single phenylalanine-to-isoleucine substitution at position 427 (F427I) in the GP2 fusion subunit of the viral envelope glycoprotein (GPC) as the sole determinant of attenuation (13, 14). The mechanism by which this substitution acts is unknown. Nevertheless, the primary reliance on the single missense mutation for attenuation raises concerns regarding the potential for reversion to virulence.

JUNV entry into the host cell is initiated by GPC binding to its cell surface receptor, transferrin receptor 1 (TfR1) (15). The virion is then internalized through endocytosis, and fusion of the viral and endosomal membranes is mediated by pH-induced conformational changes in GPC (16). Like other class I viral fusion glycoproteins, GPC is synthesized as a precursor polypeptide that is subsequently cleaved to generate the mature receptor-binding and transmembrane fusion subunits, GP1 and GP2, respectively. In addition, GPC retains a unique stable signal peptide (SSP) as a third subunit in the mature complex (17, 18) (Fig. 1). The 58-amino-acid-residue SSP contains two hydrophobic regions that span the membrane to create a hairpin structure (19). Our previous studies demonstrated that SSP interacts with GP2 to form a functional unit that senses endosomal pH and triggers the fusogenic conformational changes in GPC (20–22). Interestingly, substitutions at K33 in the ectodomain loop of SSP that abrogate

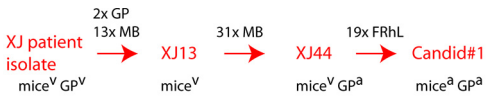

Isolate	GP1 168	GP1 186	GP1 206	GP2 427	GP2 446
XJ13	T	E	S	F	T
XJ17	A	E	S	F	T
XJ34	A	E	S	F	S
XJ39, 48	A	E	S	F	S
Candid#1	A	G	P	I	S

FIG 2 Derivation of Candid#1 (13). (Top) Passage history and selected intermediate isolates. GP, passages in guinea pigs; MB, passages in mouse brain; FRhL, passage in fetal rhesus lung epithelium cell culture. Virulence (v) or attenuation (a) in the respective species is shown below. (Bottom) Amino acid substitutions detected in GPC. Position 427 in GP2 is highlighted. The ectopically expressed MC2 GPC utilized in the present studies is identical to the XJ13 progenitor at these positions.

membrane fusion activity can be effectively complemented by mutations in GP2, including at the attenuating position 427 in Candid#1 (21). Thus, the apparent incompatibility between such K33 mutations and the wild-type F427 in pathogenic strains of JUNV may provide an evolutionary barrier against reversion of the attenuating F427I mutation in a second-generation Candid#1 vaccine.

RESULTS

The attenuating F427I mutation does not affect the expression of GPC or its membrane fusion activity. In the course of passage, Candid#1 acquired 13 amino acid substitutions, five of them in GPC (11, 13) (Fig. 2). Of the 13 substitutions, only the F427I mutation in the transmembrane domain of Candid#1 GP2 is necessary and sufficient for attenuation. This point mutation renders the pathogenic XJ13 and Romero isolates of JUNV avirulent in mouse and guinea pig models of lethal infection (13, 14). Conversely, replacement of Candid#1 GP2 with one bearing F427 creates a virulent virus (13). The other substitutions in Candid#1 are not required for attenuation but may contribute to virus fitness in cell culture and/or provide marginal support to the attenuation phenotype (14).

To better understand the molecular basis for attenuation by the F427I substitution, we introduced the I427F or F427I mutation into the respective GPCs of Candid#1 (Can) and the pathogenic MC2 isolate of JUNV (23). The GPC of MC2 is 99% identical to that of the XJ13 progenitor of Candid#1 (24) and has been extensively characterized (18, 20, 21). The parental and mutant proteins were ectopically expressed in Vero cells to assess potential changes in GPC biogenesis and membrane fusion activity. Strikingly, we found that the parental MC2 GPC accumulated to a level ~6-fold greater than that of Can GPC (Fig. 3A). This difference, however, was wholly attributable to the presence of the T168A substitution in Can GPC (Fig. 2). Replacement of alanine by threonine at this position in Can GPC restored the expression level to that of MC2 GPC, whereas a T168A mutation in MC2 GPC reduced expression to a level comparable to that of Can GPC (Fig. 3A). These observations are consistent with a previous report demonstrating that the T168A mutation, which destroys a functional glycosylation motif at N166 in GP1, reduces steady-state levels of Can GPC (25). Despite its effect on GPC expression, the T168A mutation is not directly associated with attenuation (13, 14) and in fact first arose in an early pathogenic predecessor of Candid#1 (Fig. 2). Independent of the effects of mutations at position 168, substitutions at position 427 did not significantly impact steady-state levels of GPC. Proteolytic processing to generate the mature GP1 and GP2 subunits likewise was unaffected by mutations at position 427 (Fig. 3B).

The substitution at position 427 also did not significantly impact pH-induced cell-cell fusion activity (Fig. 3C). In these studies, syncytium formation was triggered by exposure of GPC-expressing Vero cells to medium adjusted to pH 5.0. Curiously, and despite the reduction in steady-state levels due to the T168A mutation, cells expressing Can GPC were consistently more fusogenic than those expressing MC2 GPC. This difference nonetheless was modulated by substitutions at position 168 in a manner

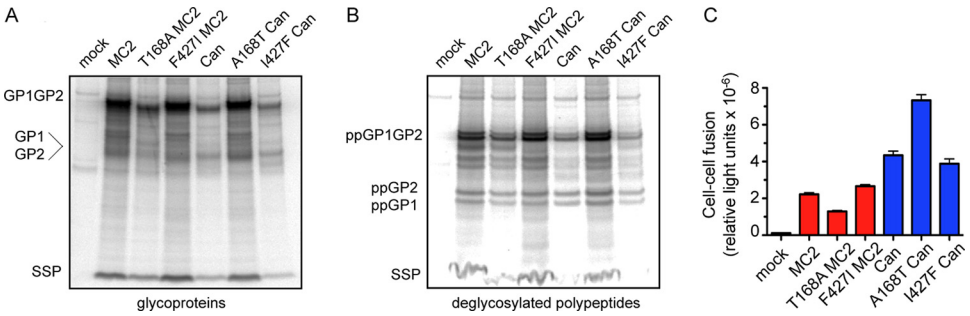

FIG 3 Effect of A168T and F427I mutations on expression and cell-cell fusion activity of ectopically expressed GPC. (A and B) Metabolically labeled Candid#1 and MC2 GPCs were immunoprecipitated from transfected Vero-76 cells using the anti-GP1 MAb BF11 and resolved using NuPAGE. The mature GP1 and GP2 subunits comigrate as glycoproteins (A) and are resolved following deglycosylation by treatment with PNGase F (B). The uncleaved GP1GP2 precursor is labeled, and deglycosylated polypeptides are indicated as pp. GPC expression was quantitated by using a Fuji FLA3000G phosphorimager and ImageGauge software. Photostimulated luminescence (PSL) values in the respective GP1GP2 precursor bands in panel A are 427,881, 174,626, 360,045, 68,087, 339,735, and 53,852. This pattern of expression was confirmed in three replicate analyses. (C) Cell-cell fusion activity of the ectopically expressed MC2 (red) and Candid#1 (blue) GPCs was triggered by exposure to medium adjusted to pH 5.0 and determined using a chemiluminescent β-galactosidase fusion reporter. Relative light units are plotted. Error bars represent the standard errors of the means from replicate fusion reactions. Complete and partial replicates of this experiment ($n > 4$) yielded concordant results. A pairwise statistical comparison using a 2-tailed Mann-Whitney analysis, as implemented in GraphPad Prism software, demonstrated that Can GPC is significantly more fusogenic than MC2 GPC ($P = 0.0002$).

consistent with changes in GPC accumulation (Fig. 3C). The molecular basis for the enhanced cell-cell fusion activity of ectopically expressed Can GPC is unclear.

Previous studies have reported that introduction of the F427I mutation into GPC of the pathogenic XJ isolate of JUNV raises the pH of membrane fusion to allow syncytium formation at neutral pH (26). Hence, we evaluated the optimal pH for cell-cell fusion by MC2 and Can GPC. The pH profiles for the two GPCs were surprisingly similar, and amino acid substitutions at position 427 had no effect on the pH of fusion (Fig. 4A). In no case did we observe syncytium formation at pH 6.0. This departure from published results (26) may reflect differences in the GPC backbone or the experimental system used.

In order to investigate this point further, we examined the sensitivity of the Candid#1 virus to pH-induced inactivation. We employed reverse genetics (27, 28) to rescue a recombinant Candid#1 virus (rCan) and subjected the virus to low pH to trigger the abortive fusogenic reorganization in GPC. Exposure to pH 5.0 abrogated the

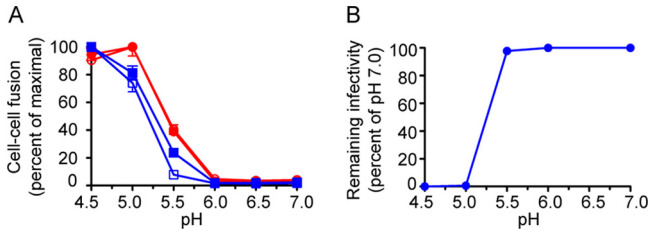

FIG 4 Attenuating F427I mutation has little or no effect on the pH of GPC fusion. (A) The pH profile for cell-cell fusion by ectopically expressed MC2 (red, closed circle) and Candid#1 (blue, closed square) GPCs was determined by varying the pH of fusion activation, as indicated. Open circle, F427I MC2 GPC; open square, I427F Can GPC. Fusion activity was normalized to the maximum value for each construct. Error bars represent the standard errors of the means from 8 replicate fusion reactions. The minimal difference in the profiles of Can and MC2 GPC was not observed in all experiments ($n = 3$), suggesting that MC2 and Can GPCs do not differ significantly in pH sensitivity. (B) rCan virus was dialyzed into weakly buffered saline at 4°C, and aliquots were diluted into sodium acetate-saline solution adjusted to the indicated pH. The final pH was confirmed in parallel dilutions without virus. Following incubation for 30 min at 37°C, the mixture was neutralized by the addition of DMEM–2% FBS and serial dilutions were used in focus-forming assays to determine the number of remaining infectious particles. Infectivity was normalized relative to that of virus treated at pH 7.0. This experiment was repeated twice using duplicate cell monolayers to determine virus titers.

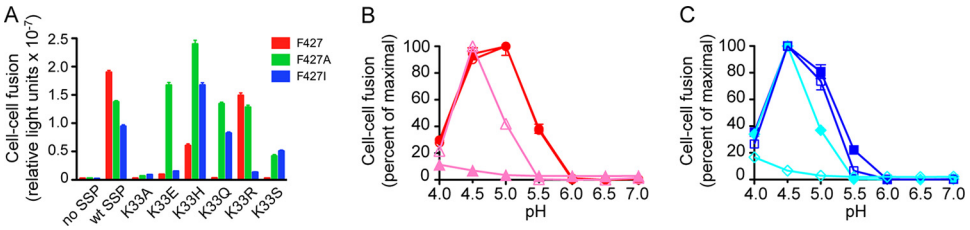

FIG 5 Attenuating F427I mutation rescues the fusion deficiency engendered by the K33S substitution. (A) MC2 GPCs were expressed in Vero cells by cotransfection of plasmids bearing SSP and the GP1GP2 precursor (fused to the conventional CD4 signal peptide). Thus, the wild-type SSP and indicated SSP mutants (K33A, E, H, Q, R, and S) were paired with the wild-type F427 and F427A and F427I mutants in GP2. Our previous studies have shown that these K33 mutants reconstitute the tripartite GPC complex comparably to the wild-type SSP (20). Cell-cell fusion activity was determined upon activation at pH 5.0. Error bars represent the standard errors of the means from 8 replicate fusion reactions. Previous studies have reported the systematic effects of charge mutations at K33 in MC2 GPC (20) and *trans*-complementation between K33Q and F427A (21). Note that K33S SSP abolishes MC2 GPC fusion activity at pH 5.0, and that fusion is restored upon pairing with either F427A or F427I. In slight contrast to results displayed in Fig. 3C, the F427I mutation in MC2 GPC resulted in an ~50% decrease in fusion activity in this study; we attribute this difference to normal variation in these assays. Overall conclusions are gleaned from multiple complete and partial replicates of the experiment. (B and C) The pH profile for cell-cell fusion by ectopically expressed GPCs bearing mutations at positions 33 and 427. Wild-type MC2 GPC (red, closed circle) and its mutants, F427I (red, open circle), K33S (pink, closed triangle), and K33S F427I (pink, open triangle), are shown in panel B. Wild-type Can GPC (blue, closed square) and its mutants, I427F (blue, open square), K33S (cyan, closed diamond), and K33S I427F (cyan, open diamond), are shown in panel C. Error bars represent the standard errors of the means from 8 replicate fusion reactions. The pattern of pH sensitivity was confirmed in three independent studies. The profiles for wild-type MC2 and Can GPC are reproduced from Fig. 4.

ability of the virus to subsequently infect Vero cells (Fig. 4B). Importantly, we found no evidence of pH-triggered inactivation at elevated pH. Collectively, our results indicate that the attenuating F427I mutation in Can GPC does not by itself impact GPC expression or its intrinsic membrane fusion activity.

The attenuating F427I substitution rescues membrane fusion activity of GPC bearing mutations at SSP K33. We have previously shown that mutations that decrease positive polarity at position K33 in SSP systematically lower the pH required to initiate membrane fusion (20) and that select alanine substitutions in GP2, including F427A, are able to restore wild-type pH sensitivity in the double mutant without themselves altering the pH of fusion (21). To determine whether the attenuating isoleucine acts similarly, we paired the F427I mutation with a series of charge mutations at K33. In these experiments, we cotransfected plasmids expressing SSP with those encoding the GP1GP2 precursor, fused to a conventional signal peptide, to reconstitute the native MC2 GPC complex (18, 29). Only the positively charged K33R and K33H substitutions yield significant fusion activity when paired with wild-type GP1GP2 (20). Pairing with F427A GP1GP2 rescued the fusion activity of the otherwise defective K33E, K33Q, and K33S mutants (Fig. 5A) (21). The F427I substitution also was able to restore fusion activity to the K33Q and K33S mutants but not to K33E GPC. Unexpectedly, the F427I substitution abolished the fusion activity of K33R GPC. Thus, the pattern of complementation by F427I differs from that of F427A. More broadly, these results suggest that the sidechain at position 427 participates in the control of fusion activation and, by extension, that the attenuating mutation acts through the GPC fusion machinery, albeit in a manner that is not detected in our studies of the ectopically expressed protein.

F427I partially restores the wild-type pH profile of K33S GPC. We were particularly interested in understanding the interplay between K33S and the attenuating F427I mutation. As anticipated, complementation of the K33S defect was associated with a shift in the pH profile toward the wild-type pH optimum. Whereas K33S MC2 GPC required exposure to pH 4.0 in order to achieve even a minimal level of cell-cell fusion, the complementing F427I mutation increased fusion activity and shifted the optimum pH to 4.5 (Fig. 5B). The residual depression in the pH of fusion relative to the wild-type MC2 GPC (pH~5.0) points to incomplete complementation. K33S Can GPC, containing the endogenous F427I mutation, displayed a similar residuum of pH depression relative

TABLE 1 Nucleotide changes in K33S-GPC rCan upon serial passage in the presence and absence of 1 mM AmCl

	Stock		p11 no AmCl		p21 AmCl	
Nucleotide(s) (nt)	nt change[a] (% reads)	Amino acid change	nt change (% reads)	Amino acid change	nt change (% reads)	Amino acid change
S RNA						
5′ end	1–8 missing		1–8 missing		1–8 missing	
186–202; 217	K33S oligonucleotide[b] (≥98)		K33S oligonucleotide (≥98)		K33S oligonucleotide (≥98)	
590					G→A (55)	GP1 A168T
863–883					Delete codons T_{259}DSSGKD$_{265}$	GP2 ΔFP
1127			A→T (88)	GP2 I347F		
1146					T→C (39)	GP2 V353A
1401			T→C (19)	GP2 F438S		
1535			A→G (35)	GP2 R483G		
1655					G→A (51)	NP A560T
2382					T→C (40)	NP S317 silent
3406 (3′-UTR)	A→T (56)				A→T (38)	
3′ end			3407–3413 missing		3411–3413 missing	
L RNA						
5′ end	1–4 missing				1–5 missing	
150					G→A (90)	Z A23T
4687					A→G (49)	L N800D
3′ end			7111–7114 missing		7111–7114 missing	

[a]Changes present in ≥10% of reads relative to the sequence of reverse genetics plasmids used to construct rCan viruses (28). The raw RNA-Seq data originally were aligned to Candid#1 S and L RNA reference genomes (AY746353.1 and AY746354.1, respectively).

[b]In addition to the K33S mutation, the mutagenic oligonucleotide introduced 4 synonymous nucleotide changes and an I35V change (see Materials and Methods and the text).

to the parental Can GPC (Fig. 5C). Furthermore, introducing the I427F mutation into K33S Can GPC reproduced the fusion defects seen with K33S MC2 GPC. These findings highlight the collaboration between SSP and GP2 in regulating the pH of fusion activation as well as the complex interplay between the attenuating F427I mutation and K33S in SSP.

K33S-F427I epistasis in a recombinant rCan virus. The genetic interactions between specific sidechains at positions 33 in SSP and 427 in GP2 suggest a means of designing an evolutionary barrier against Candid#1 reversion to the pathogenic F427 genotype. As F427 renders certain K33 mutants unable to mediate membrane fusion at endosomal pH, we surmised that reversion would be lethal in a Candid#1 virus bearing the appropriate K33 mutation. To test this notion, we engineered the K33S substitution into rCan using reverse genetics (27, 28). This mutation was chosen due to the severity of the fusion defect in the presence of F427 (20) and to take advantage of the fact that two nucleotide changes would be required for back-mutation to wild-type K33. In addition to the K33S substitution, the mutagenic oligonucleotide introduced four synonymous nucleotide changes and replaced isoleucine at position 35 with valine found in MC2 GPC (see Materials and Methods). The latter substitution does not impact rCan titers or focus morphology (not shown). To simplify subsequent designations of rCan mutants, the substitution at position 35 will not be explicitly noted. The K33S-GPC rCan mutant was readily rescued using reverse genetics, and next-generation RNA sequencing (RNA-Seq) analysis confirmed retention of the K33S substitution and the absence of any unintended changes in GPC or other coding regions (Table 1). The sole variant was a previously noted (28) A-to-T transversion in the 3′-untranslated region (UTR) of the S RNA in 56% of reads. Although K33S-GPC rCan produced smaller foci than the parental rCan upon growth under agarose (Fig. 6A), the foci tended to stain more deeply using an anti-nucleoprotein (NP) MAb, indicative of robust virus production. Indeed, the two viruses achieved comparable endpoint titers after expansion in Vero cells (not shown). To assess growth kinetics in detail, Vero cell cultures were infected at a low multiplicity of infection (MOI) of 0.01, and virus growth was measured by sampling the culture supernatant over the course of 72 h. Virus particle production was

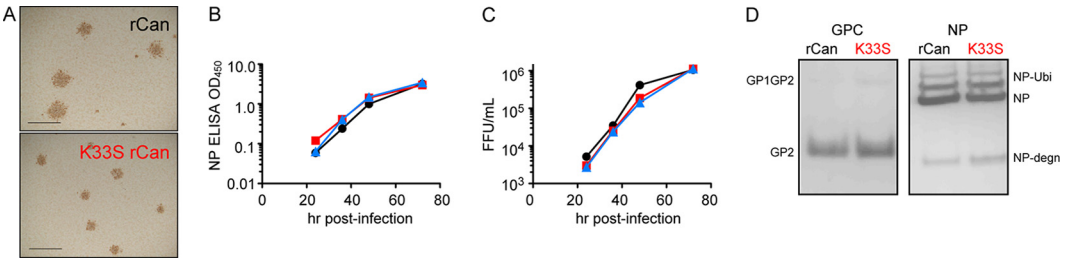

FIG 6 Growth and biochemical properties of rCan viruses. (A) Photomicrograph of foci produced under agarose by parental (top) and K33S-GPC (bottom) rCan viruses. Foci were immunochemically stained using the anti-NP MAb AG12. Scale marker, 2 mm. (B and C) Growth kinetics following low-multiplicity infection (MOI, 0.01) of Vero cells with parental rCan (black circles), K33S-GPC rCan (red squares), and K33S/A168T/ΔFP-GPC rCan (blue triangle). Cell culture supernatants were harvested at indicated times, and virion accumulation was assessed by NP ELISA (B) and by enumeration of focus-forming units (FFU) (C). Input viral titers were confirmed contemporaneously. The relative specific infectivity of the virus was calculated as the ratio of FFU/ml and NP ELISA values. Virus spread through the culture was qualitatively assessed by immunochemical staining of the monolayer; all viruses spread comparably, and cultures were completely infected by 72 h postinfection. (D) Purified rCan and K33S-GPC rCan virions harvested at 48 h were subjected to immunoblot analysis using either GP2-directed MAbs G3 and G5 (38) or the NP-directed MAb AG12. Only the proteolytically mature GPC is incorporated into virions. More slowly migrating NP bands have been shown to represent ubiquitinated forms of the protein (NP-Ubi; unpublished data). A frequently observed NP degradation product is indicated as NP-degn. The results presented in this figure were representative of three replicate studies.

quantitated by using an NP enzyme-linked immunosorbent assay (ELISA) (Fig. 6B), and the infectious virus titer was determined by focus formation (Fig. 6C). Despite the difference in focal size, the growth curves of the K33S-GPC and parental rCan viruses were quite similar. A comparison of the ratio of focus-forming units (FFU) to virion NP revealed that the specific infectivities of the two viruses were also comparable (4.7×10^5 versus 5.3×10^5 arbitrary units, respectively). In keeping with its robust infectivity, GPC incorporation into K33S-GPC rCan virions was similar to that of the parental virus (Fig. 6D). Thus, K33S-GPC rCan manifests little or no deficit in infectivity relative to that of rCan.

To determine whether K33S-GPC rCan retains the residual depression in the pH of fusion noted in the ectopically expressed mutant, we evaluated its sensitivity to the lysosomotropic agent ammonium chloride (AmCl). We reasoned that the residual reduction in optimal pH would result in increased sensitivity to the pH-elevating effects of AmCl. Indeed, K33S-GPC rCan was significantly more sensitive to AmCl than the rCan parent (Fig. 7A). The presence of 1 mM AmCl reduced K33S-GPC rCan infectivity by >95%, whereas the parental rCan was inhibited by 60%. Taken together, our results

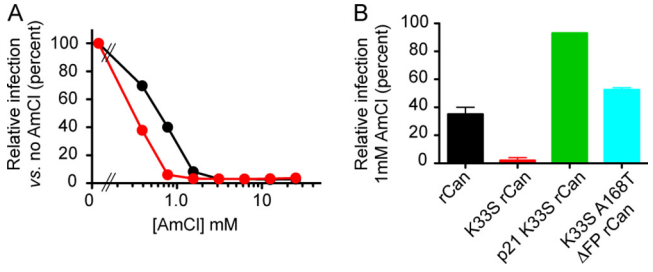

FIG 7 AmCl sensitivity of rCan viruses. (A) Parental (black circle) and K33S-GPC rCan (red circle) viruses were used to infect Vero cell monolayers grown in the continued presence of the indicated concentrations of AmCl. Inocula were removed after 2 h, and cultures were continued for 24 h. Cell monolayers then were solubilized in buffer containing 1% Triton, and NP production was determined by ELISA. Infection was normalized relative to viral growth in the absence of AmCl. Error bars from 11 replicate ELISA wells are not visible. (B) Sensitivity of rCan viruses following serial passage in medium containing 1 mM AmCl was assessed as described above, albeit at a fixed concentration of 1 mM AmCl. Viruses tested are rCan (black), K33S-GPC rCan (red), p21 K33S-GPC rCan stock obtained after 21 serial passages (green), and K33S/A168T/ΔFP-GPC rCan engineered to match p21 stock (blue). Error bars indicate the standard errors of the means from 2 replicate ELISA wells. Results presented in this figure are representative of at least two independent experiments.

TABLE 2 Nucleotide changes in parental rCan upon serial passage in the presence and absence of 1 mM AmCl

	Stock		p10 no AmCl		p21 AmCl	
Nucleotide (nt)	nt change[a] (% reads)	Amino acid change	nt change (% reads)	Amino acid change	nt change (% reads)	Amino acid change
S RNA						
5′ end	1–8 missing		1–8 missing		1–8 missing	
311					T→C (63)	GP1 F75L
977					C→T (25)	GP2 H297Y
1367					A→T (94)	GP2 I427F
1793					A→T (27)	NP T514S
2217					C→T (38)	NP D372 silent
3406 (3′-UTR)			A→T (67)		A→T (53)	
3′ end					3413 missing	
L RNA						
5′ end	1–4 missing		1–5 missing		1–5 missing	
150					G→A (65)	Z A23T
3′ end	7114 missing		7109–7114 missing		7111–7114 missing	

[a]Changes present in ≥10% of reads relative to the sequence of reverse genetics plasmids used to construct rCan viruses (28). The raw RNA-Seq data originally were aligned to Candid#1 S and L RNA reference genomes (AY746353.1 and AY746354.1, respectively).

indicate that the epistatic interaction between K33S and F427I described in ectopically expressed GPC is recapitulated in the rCan mutant.

K33S-GPC rCan retains K33S and F427I upon prolonged passage in Vero cells. As an RNA virus, Candid#1 exists as a quasispecies that contains genetic variants that have been shown to give rise to clonal isolates of differing virulence (30, 31). Nonetheless, the attenuated phenotype of Candid#1 appears to be stable in research laboratories and throughout its limited use as a vaccine. To formally assess the genetic stability of the parental rCan, we passaged the virus twice weekly in Vero cells, adjusting the inoculum to maintain a relatively low MOI and extensive spread over the course of 3 to 4 days of culture. After 10 passages, the p10 virus was subjected to RNA-Seq. Other than the previously noted A-to-T transversion in the S RNA 3′-UTR (28), no additional nucleotide changes were identified (Table 2). The stability of rCan perhaps is not surprising because Candid#1 had been extensively passaged in Vero cells.

To characterize the genetic stability of K33S-GPC rCan, we passaged the virus in parallel with the parental rCan. RNA-Seq analysis was performed after 11 twice-weekly passages. Notably, this analysis confirmed retention of the K33S and F427I mutations (≥98% of reads each) (Table 1). We also identified the following novel mutations in GP2: I347F, F438S, and R483G in 88%, 19%, and 35% of reads, respectively. Interestingly, mutations at positions 347 and 438 have been shown to impact SSP-GP2 interactions similarly to those at position 427. For example, F438I also complements the fusion deficiency in K33Q GPC (21), and F427A, I347A, and F438I all engender resistance to small-molecule fusion inhibitors that bind at the SSP-GP2 interface (32, 33). The R483G mutation disrupts a putative dibasic trafficking signal in the cytoplasmic C-terminal region of GP2 (34). No additional changes were noted elsewhere in the genome. While the effects of these novel mutations on GPC structure and function remain to be characterized, the retention of K33S and F427I speaks to the genetic stability of the complementing mutations.

Determinants of AmCl sensitivity in K33S-GPC rCan. Incomplete complementation of the K33S defect by I427 in K33S-GPC rCan results in an increased sensitivity to AmCl (Fig. 7B). Hence, we reasoned that growth of K33S-GPC rCan in the presence of AmCl would select for secondary genetic changes that alter the pH of fusion. To this end, we passaged K33S-GPC rCan in the continued presence of 1 mM AmCl, using the strategy described above. As shown in Fig. 7B, the virus population after 21 passages (p21) was now resistant to the inhibitory effects of 1 mM AmCl. RNA-Seq analysis revealed that both K33S and F427I mutations were retained in ≥98% of reads (Table 1). In addition, several novel mutations were noted in GPC. Interestingly, we found that

A168 had reverted to the wild-type T168 in 55% of reads. This back-mutation was previously noted upon serial passage of the ΔG2-GPC rCan mutant in standard cell culture medium (28), suggesting that the presence of the N166 glycan enhances virus fitness in cell culture. The V353A substitution in GP2 (39% of reads) is also noteworthy due to its proximity to the I347F change noted upon passage of K33S-GPC rCan in the absence of AmCl. These positions lie adjacent to and within the HR1d segment of the N-terminal heptad-repeat helix in the prefusion form of GPC (35, 36) and thus may be involved in conformational changes associated with membrane fusion. Most remarkably, we also identified a precise 7-amino-acid deletion (96% of reads) between the N-terminal and internal segments of the bipartite fusion peptide of GP2 (37, 38). The missing residues form a short α-helical region in the prefusion structure of lymphocytic choriomeningitis virus GPC (35), and their absence would be expected to disrupt fusion peptide function. Nonetheless, the p21 virus, and subsequently engineered rCan variants bearing the fusion-peptide deletion (ΔFP; see below), were indeed viable. RNA-Seq also revealed one mutation each in NP, L polymerase, and the Z matrix protein (Table 1). The A23T mutation in Z lies within the highly variable and unstructured N-terminal region whose function is unknown (39, 40). Retention of both K33S and F427I mutations, despite prolonged passage, is consistent with important evolutionary constraints imposed by epistasis.

Serial passage of the parental rCan virus in AmCl results in complete reversion to F427. In parallel, we also passaged the parental rCan virus in the presence of 1 mM AmCl and analyzed the p21 virus population using RNA-Seq. Several amino acid substitutions were identified throughout the genome (Table 2), but the one that captured our attention was the unexpected back-mutation to the pathogenic F427 genotype in 94% of reads. In addition, we found two other missense mutations in GPC and one in NP, as well as the A23T substitution in Z noted in the similarly passaged K33S-GPC rCan (Table 2).

The finding that passage of rCan in the presence of AmCl leads concomitantly to reversion and decreased sensitivity to the effects of AmCl provides further evidence for an association between the attenuating F427I mutation and the pH-dependent process of virus entry. The experiment also indicates that novel growth conditions can exert a selective force on rCan to accelerate reversion to the pathogenic F427 genotype. As such, our failure to observe reversion in the similarly passaged K33S-GPC rCan provides supportive evidence that epistasis between K33S and F427I can indeed create an evolutionary barrier against the emergence of pathogenic rCan revertants.

rCan variants bearing the fusion peptide deletion are viable. As fusion peptides are generally highly sensitive to mutation (37, 38), we were intrigued that a K33S-GPC rCan variant bearing the 7-amino-acid ΔFP deletion was not only viable but sufficiently robust to become fixed in the p21 population. Indeed, retrospective Sanger sequence analysis of the GPC open reading frame in intermediate virus populations revealed evidence of the ΔFP deletion by the fifth passage, prior to the emergence of the A168T mutation (not shown). To reconfirm the viability of a virus containing the deletion, we constructed an rCan variant containing only the ΔFP deletion. Although ΔFP-GPC rCan was readily rescued and grew to titers comparable to those of the parental rCan, serial passage in standard cell culture medium yielded a mixture of differently sized foci (not shown). Sanger sequencing of the GPC open reading frame revealed the emergence of a single mutation, I427F (Fig. 8A). The mutation was present in ~50% of the virus population after five passages, and reversion was complete after 10 passages. The I427F mutation also arose upon passage in the presence of 1 mM AmCl (Fig. 8A). We conclude that the ΔFP deletion is highly detrimental on its own and that back-mutation to F427 offers an accessible evolutionary path for enhancing viral fitness.

The genetic instability of ΔFP-GPC rCan suggested that one or more mutations in the p21 K33S-GPC rCan virus population contributed to the emergence of the deletion. Hence, we reconstructed a K33S-GPC rCan variant bearing ΔFP and A168T. The triple mutant virus was viable and manifested a specific infectivity similar to that of the

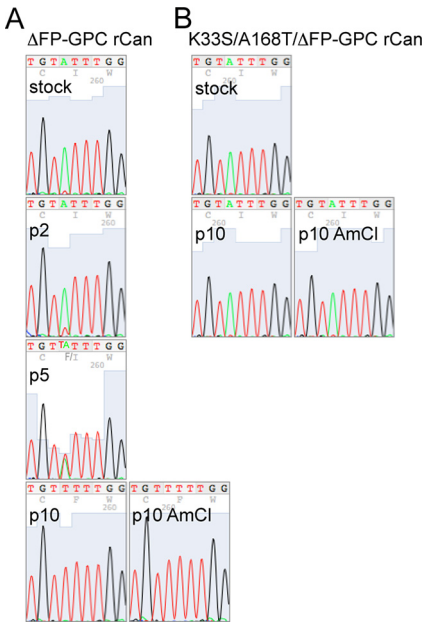

FIG 8 ΔFP-GPC rCan undergoes I427F reversion upon serial passage, whereas K33S/A168T/ΔFP rCan does not. ΔFP-GPC rCan (A) and K33S/A168T/ΔFP rCan (B) were serially passaged 10 times in the presence or absence of 1 mM AmCl. Virion RNA was prepared after 2, 5, and 10 passages, and the RT-PCR product of the GPC open reading frame was subjected to Sanger sequencing. The chromatograms reveal the emergence of the I427F mutation (ATT to TTT) in the former but not latter virus. No additional changes in GPC were noted.

K33S-GPC parent (3.9×10^5 versus 4.7×10^5 arbitrary units, respectively; described above). Moreover, the mutant displayed a substantial increase in its resistance to AmCl (Fig. 7B). In contrast to ΔFP-GPC rCan, the triple mutant virus was genetically stable upon serial passage in Vero cells, with or without the addition of 1 mM AmCl. Focus size was unchanged and Sanger sequencing of the GPC gene revealed complete retention of I427 after 10 passages (Fig. 8B). No additional sequence changes were detected in GPC. This degree of genetic stability is consistent with fixation of the ΔFP deletion in the original p21 population. Furthermore, as the original quasispecies contained the A168T mutation in only 55% of genomes, we infer that the stability of the ΔFP deletion is dependent on K33S, if only by precluding facile reversion to F427.

DISCUSSION

Live-attenuated viral vaccines confer strong durable protection against infection and disease. However, these products also carry the intrinsic risk of reversion to virulence. This factor weighs heavily in risk-benefit calculations performed by regulatory agencies, vaccine manufacturers, and public health officials. In response to an emerging epidemic of Argentine hemorrhagic fever in the 1960s, the Argentine government and its partners developed an attenuated strain of JUNV (Candid#1) that is still used in Argentina to immunize high-risk agricultural workers (5). Despite recent concerns regarding the potential for natural and intentional spread of JUNV beyond Argentina (https://www.niaid.nih.gov/research/emerging-infectious-diseases-pathogens), the Candid#1 vaccine is not licensed for use in the United States. One hindrance to licensure lies in the fact that Candid#1 attenuation is dependent on a single F427I mutation in the GP2 subunit of GPC. In this study, we have demonstrated that revertants at this position can emerge upon serial passage of Candid#1 in cell culture. Growth in the presence of a mildly inhibitory concentration of AmCl was sufficient to select for reversion in rCan, and serial passage in routine cell culture resulted in reversion of the ΔFP-GPC rCan mutant. Thus, reversion to F427 provides a facile evolutionary pathway to enhance viral fitness under conditions that perturb the

existing quasispecies. Growth of the virus during vaccine manufacture, or upon expanded use in humans, may similarly drive reversion of the attenuating mutation.

Here, we identify an intragenic epistasis within Can GPC that can be exploited to establish an evolutionary barrier against reversion of the attenuating mutation. In particular, we show that the K33S mutation in SSP, which abolishes cell-cell fusion activity when paired with F427 present in pathogenic JUNV isolates, can be complemented by the attenuating F427I substitution in ectopically expressed GPC. This epistatic interaction is recapitulated in the intact virus to support robust replication of K33S-GPC rCan. We further demonstrate that rCan variants containing the K33S mutation do not revert upon serial passage in cell culture under conditions that drive reversion in viruses bearing the wild-type K33. If genetic stability is maintained through scale-up and development, this epistasis may provide the basis for a safe and effective second-generation rCan vaccine.

The mechanism by which the F427I mutation mediates attenuation remains obscure. Our genetic and biochemical studies of ectopically expressed GPC reveal no significant differences between F427- and I427-containing proteins in either the Can or MC2 GPC background. In contrast to a previous report (26), the activity and optimal pH of GPC-mediated cell-cell fusion are unaffected by the F427I substitution. Our results are consistent with those of Seregin et al. demonstrating comparable growth kinetics in the cognate viruses (14).

It is notable that residues at the site of attenuation in GP2 interact with K33 in SSP to modulate the pH at which membrane fusion is activated. Mutations at these positions also modulate GPC sensitivity to small-molecule fusion inhibitors that bind at the SSP-GP2 interface and antagonize pH-induced fusion activation (32, 33, 41). Despite our inability to detect functional differences between ectopically expressed GPCs bearing either F427 or I427, this analysis no doubt fails to incorporate elements that are nonetheless critical for virus-cell entry. For example, GPC-mediated cell-cell fusion is largely independent of the TfR1 cell surface receptor required for virus entry. Cell-cell fusion also bypasses endosomal trafficking, thereby precluding potential interactions with any endosomal receptors and proteases (42). Furthermore, it is unknown if and how virion assembly affects GPC function. Thus, it remains plausible that attenuation in rCan is mediated through effects on the membrane fusion machinery that are not apparent in studies of the ectopically expressed protein.

Despite differences in receptor requirements and entry pathways (43, 44), the New World and Old World arenaviruses share a GPC architecture (35, 45). Indeed, several classes of small-molecule fusion inhibitors target both groups of viruses (41, 46). While some inhibitors are selective for a single group of viruses, sensitivity can be switched by mutation at the K33 site (32). Thus, it is likely that the epistatic interactions discovered in JUNV GPC are also present in LASV GPC. Hence, analogous attenuation strategies may be useful in designing a live-attenuated viral vaccine to conquer this important disease.

MATERIALS AND METHODS

Molecular reagents, cells, and antibodies. Candid#1 reverse genetics plasmids mPol-I-Sag (#30), mPol-I-Lag (#35), pC-L, and pC-NP were kindly provided by Juan Carlos de la Torre (Scripps Research Institute, La Jolla, CA) and Slobodan Paessler (University of Texas Medical Branch, Galveston, TX) (27). The GPC open reading frame from mPol-I-Sag was subcloned for ectopic expression in pcDNA3.1-based plasmids by using PCR. Similar plasmids encoding GPC derived from the pathogenic MC2 isolate of JUNV (GenBank accession number P26313) (23) have been described previously (18, 47). For some studies, the separate open reading frames of SSP and the GP1GP2 precursor (fused to the conventional signal peptide of human CD4) were coexpressed on separate plasmids to reconstitute the intact GPC (18, 29). BHK-21 and Vero-76 cells were obtained from the ATCC. Monoclonal antibodies (MAbs) directed to JUNV GP1 (BF11) and nucleoprotein (NP; AG12 and AA10) (9) were obtained through the NIAID Biodefense and Emerging Infections Research Program (BEI Resources). The GP2-directed MAbs G3 and G5 (38) used in immunoblot experiments were kindly provided by the Public Health Agency of Canada (Winnipeg, MB).

Ectopic expression of GPC. GPC open reading frames were expressed through Lipofectamine 2000 (Life Technologies)-mediated transfection of Vero cells using the minimal bacteriophage T7 promoter of the pcDNA3.1 plasmids and T7 polymerase, provided by concurrent infection with the recombinant vaccinia virus vTF7-3 (48) as previously described (18, 47). Cells were grown in Dulbecco's modified Eagle medium (DMEM) containing L-glutamine, penicillin-streptomycin, and 10% fetal bovine serum (FBS), all from Life Technologies, and 10 μM cytosine arabinoside (araC) was added to limit vaccinia virus

replication and cytopathic effect. Cells expressing GPC were metabolically labeled using [^{35}S]methionine/cysteine (EasyTag Express; Perkin-Elmer), and immunoprecipitation was performed using the GP1-directed MAb BF11 (47). Proteins were resolved by reducing SDS-PAGE using NuPAGE 4 to 12% Bis-Tris gels (Life Technologies). Radiolabeled GPC was quantitated using a Fuji FLA 3000G phosphorimager and the Profile tool in ImageGauge software (Fuji). In some experiments, immunoprecipitated glycoproteins were deglycosylated using PNGase F (New England BioLabs). Mutations were generated using QuikChange mutagenesis (Stratagene), and the intended sequences were confirmed by DNA sequence analysis using an ABI 3130 genetic analyzer (Applied Biosystems).

GPC-mediated cell-cell fusion. A vaccinia virus-based β-galactosidase fusion reporter assay was used to assess the cell-cell fusion activity of ectopically expressed GPC as previously described (21, 32). In brief, Vero cells expressing GPC were mixed with target Vero cells infected with the vCB21R-lacZ vaccinia virus carrying the β-galactosidase gene under the control of a T7 promoter (49) and grown in the presence of 100 μg rifampin/ml. Both araC and rifampin were present in the coculture to prevent cross-infection. Cell-cell fusion was initiated by exposing the coculture to medium buffered either to pH 5.0 in the standard assay or to a range of pHs (4.5 to 7.0) to assess the pH profile for fusion activity (21, 32). Fusion-induced expression of the β-galactosidase reporter was assessed by chemiluminescence using the Galactolite plus substrate (Applied Biosystems) and a SpectraMax L microplate luminometer (Molecular Devices).

Reverse genetics methodology. Recombinant Candid#1 viruses were generated as previously described (27, 28). In brief, BHK-21 cells were cotransfected with the two antigenome plasmids mPol-I-Sag and mPol-I-Lag and with plasmids expressing the viral polymerase and nucleoprotein (pC-L and pC-NP, respectively) to initiate replication of the transcribed genomic RNAs. The rescued rCan viruses were subsequently expanded in Vero cells, and virus stocks were prepared from freeze-thawed cells and culture supernatant. All studies using recombinant Candid#1 viruses were approved by the University of Montana Institutional Biosafety Committee and performed using biosafety level 2+ (BSL2+) operations.

A mutagenic oligonucleotide previously used to generate the K33S mutant of MC2 GPC (5′-GCA GTC AGT CTC ATT GCC ATC ATT *AGC* GGc *gTc* GTa AAC cTG TAC AAA AGT GGT TTg TTC C-3′) (20) was used to introduce this mutation into rCan GPC. In addition to the K33S change (indicated in uppercase italics), this oligonucleotide also introduced four synonymous nucleotide changes (lowercase roman) and replaced isoleucine at position 35 with the valine found in MC2 GPC (lowercase italics). The latter substitution does not appear to impact the behavior of either ectopically expressed Can GPC or rCan viruses (not shown). Additional oligonucleotides were used to introduce the following mutations into K33S-GPC rCan: A168T (5′-CCA CCA TTT CTG TGT AGG AAC CGT *ACA* AAG ACA GAA GGC TTC ATC TTT CAA GTC-3′) and ΔFP (5′-CTT CCA AGG AGG TCT TTA AAA GCA TTC TTT TCC TGG TCT CTG ACC CCT GGA GGC TAT TGT CTA GAA GAG TGG-3′).

Virus characterization. Viral titers and focal growth morphology were determined by incubating serial dilutions of the virus in duplicate with Vero cell monolayers prepared in 6-well culture dishes containing DMEM with 2% FBS. Following a 1-h incubation, the medium was removed and replaced with a 1:1 mix of 2× MEM without phenol red (Life Technologies) and 1% LMP agarose (Life Technologies). Cultures were continued for 4 to 5 days and subsequently fixed by the addition of an equal volume of Dulbecco's phosphate-buffered saline (DPBS) containing 4% paraformaldehyde. Upon removal of the agarose overlay, dishes were immunochemically stained using the MAb AG12 and a secondary horseradish peroxidase (HRP)-conjugated anti-mouse IgG antibody and diaminobenzidine (DAB) substrate.

Virion NP content was quantitated by sandwich ELISA using MAb AG12 for capture and the noncompeting biotinylated MAb AA10 for detection (50). MAb AA10 was biotinylated using EZ-Link Sulfo-NHS-LC-Biotin (Life Technologies) and detected with NeutrAvidin-HRP (Pierce) and Sure Blue reagent (KPL). Optical densities were measured at 450 nm using a VMax microplate reader (Molecular Devices). The assay is linear with respect to NP concentration to optical densities of $\geq$3.0.

In some studies, virions were partially purified from cleared cell culture supernatants by centrifugation through a cushion of 20% sucrose in DPBS. For immunoblot analysis, virion pellets were solubilized in NuPAGE LDS sample buffer with reducing agent (Life Technologies), and proteins were resolved by using 4 to 12% NuPAGE gels (Life Technologies). Proteins then were transferred to Novex polyvinylidene difluoride (PVDF) membranes (Life Technologies) and probed using either MAbs G3 and G5 (GPC) or AG12 (NP). Bands were visualized via a secondary HRP-conjugated anti-mouse IgG antibody and ECL 2 Western blotting substrate (Pierce). Chemifluorescence was quantitated using a Fuji FLA 3000G imager and ImageGauge software (Fuji).

RNA from virions and infected cells was prepared using TRIzol reagent (Ambion) for Sanger sequencing of the GPC open reading frame. Reverse transcription-PCR (RT-PCR) was performed as previously described (28) using the rCan 5′-UTR (5′-GGGGATCCTAGGCGATTTTGGTTACGC-3′) and rCan GPC 2 (5′-CCTTCTGTCTTTGCACGGTTCC-3′) oligonucleotide primers.

Virus growth curves. Virus growth curves were initiated by infection of Vero cells at a multiplicity of 0.01 in replicate 6-cm culture dishes using medium containing 2% FBS. The virus was removed after 1 h and cultures were continued in the same medium. Over the course of 72 h, dishes were harvested and cell culture supernatants were used to assess infectious virus production (focus-forming units) and nucleoprotein content (ELISA) as described above. Cell monolayers were fixed with methanol-acetone and immunochemically stained using the MAb AG12, HRP-conjugated secondary antibody, and DAB substrate in order to qualitatively assess virus spread in the culture.

Serial passage of rCan viruses. Viruses were subjected to serial passage in cell culture to identify evolutionary changes. Cell culture supernatants were transferred twice weekly onto fresh Vero cells in 10-cm culture dishes. The volume of each inoculum (nominally 1 ml) was adjusted based on apparent cytopathic effect to maintain a relatively low multiplicity of infection (MOI) and extensive spread over the

course of 3 to 4 days of culture. The latter was confirmed by immunochemical staining of the monolayer. In some studies, the growth medium was supplemented throughout with 1 mM AmCl.

Next-generation sequencing of virion RNAs. Virion RNA was prepared from cell culture supernatants and provided to the Yale Center for Genome Analysis (Yale School of Medicine) for library construction and deep sequencing using an Illumina HiSeq 2000 instrument as previously described (28). In brief, RNA was depleted of rRNA molecules using the Ribo-Zero Gold kit (Epicentre) and then sheared by incubation at 94°C. Following first-strand synthesis with random primers, second-strand synthesis was performed with dUTP for generating a strand-specific sequencing library. The library then was end repaired and A-tailed, and adapters were ligated prior to second-strand digestion using uracil-DNA glycosylase. Libraries were quantified by quantitative RT-PCR (KAPA Biosystems), and the insert size distribution was determined with LabChip GX. Samples were multiplexed (8×) and loaded onto Illumina version 3 flow cells at a concentration that yields 170 to 200 million passing filter clusters per lane. Samples were sequenced using a 75-bp paired-end strategy on an Illumina HiSeq 2000 according to Illumina protocols. Signal intensities were converted to individual base calls during the run using the system's real-time analysis (RTA) software.

The raw data were provided as fastq files to Sijung Yun (Yotta Biomed, LLC) for bioinformatics analysis. Read qualities were checked using FastQC software (http://www.bioinformatics.babraham.ac.uk/projects/fastqc/). The reads were aligned to the reference Candid#1 S and L RNA genomes (GenBank accession numbers AY746353.1 and AY746354.1, respectively) using BWA (version 0.7.8-r455) with the BWA-MEM algorithm (51). Variants were called using SAMtools mpileup and bcftools (52). The Broad Institute Integrated Genomics Viewer (IGV) (53) was used for further review and analysis of sequence variation. Preexisting sequence variations in the original reverse genetic plasmids were noted (28) and excluded from this analysis.

ACKNOWLEDGMENTS

We are indebted to Juan Carlos de la Torre (Scripps Research Institute, LA Jolla, CA) and Slobodan Paessler (University of Texas Medical Branch, Galveston, TX) for providing the Candid#1 reverse genetics plasmids and laboratory protocols. We are also grateful to the Yale Center for Genome Analysis (Yale School of Medicine) and Sijung Yun (Yotta Biomed, LLC, Bethesda, MD) for next-generation sequencing and bioinformatics analysis, respectively. Monoclonal antibodies were obtained from BEI Resources (NIAID Biodefense and Emerging Infections Research Program) and the Public Health Agency of Canada (Winnipeg, MB).

This work was supported by U.S. National Institutes of Health research grants AI074818 and AI119803 to J.H.N. The funders had no role in study design, data collection and interpretation, or the decision to submit the work for publication.

REFERENCES

1. Peters CJ. 2002. Human infection with arenaviruses in the Americas. Curr Top Microbiol Immunol 262:65–74.
2. McCormick JB, Fisher-Hoch SP. 2002. Lassa fever. Curr Top Microbiol Immunol 262:75–109.
3. McCormick JB, Webb PA, Krebs JW, Johnson KM, Smith ES. 1987. A prospective study of the epidemiology and ecology of Lassa fever. J Infect Dis 155:437–444. https://doi.org/10.1093/infdis/155.3.437.
4. Delgado S, Erickson BR, Agudo R, Blair PJ, Vallejo E, Albariño CG, Vargas J, Comer JA, Rollin PE, Ksiazek TG, Olson JG, Nichol ST. 2008. Chapare virus, a newly discovered arenavirus isolated from a fatal hemorrhagic fever case in Bolivia. PLoS Pathog 4:e1000047. https://doi.org/10.1371/journal.ppat.1000047.
5. Enria DA, Barrera Oro JG. 2002. Junin virus vaccines. Curr Top Microbiol Immunol 263:239–261.
6. McKee KT, Jr, Oro JG, Kuehne AI, Spisso JA, Mahlandt BG. 1993. Safety and immunogenicity of a live-attenuated Junin (Argentine hemorrhagic fever) vaccine in rhesus macaques. Am J Trop Med Hyg 48:403–411. https://doi.org/10.4269/ajtmh.1993.48.403.
7. Maiztegui JI, McKee KT, Jr, Barrera Oro JG, Harrison LH, Gibbs PH, Feuillade MR, Enria DA, Briggiler AM, Levis SC, Ambrosio AM, Halsey NA, Peters CJ. 1998. Protective efficacy of a live attenuated vaccine against Argentine hemorrhagic fever. AHF Study Group. J Infect Dis 177:277–283. https://doi.org/10.1086/514211.
8. Enria DA, Briggiler AM, Fernandez NJ, Levis SC, Maiztegui JI. 1984. Importance of dose of neutralising antibodies in treatment of Argentine haemorrhagic fever with immune plasma. Lancet ii:255–256.
9. Sanchez A, Pifat DY, Kenyon RH, J PC, McCormick JB, Kiley MP. 1989. Junin virus monoclonal antibodies: characterization and cross-reactivity with other arenaviruses. J Gen Virol 70:1125–1132. https://doi.org/10.1099/0022-1317-70-5-1125.
10. Enria DA, Briggiler AM, Sánchez Z. 2008. Treatment of Argentine hemorrhagic fever. Antiviral Res 78:132–139. https://doi.org/10.1016/j.antiviral.2007.10.010.
11. Albariño CG, Ghiringhelli PD, Posik DM, Lozano ME, Ambrosio AM, Sanchez A, Romanowski V. 1997. Molecular characterization of attenuated Junin virus strains. J Gen Virol 78:1605–1610. https://doi.org/10.1099/0022-1317-78-7-1605.
12. Goni SE, Iserte JA, Stephan BI, Borio CS, Ghiringhelli PD, Lozano ME. 2010. Molecular analysis of the virulence attenuation process in Junin virus vaccine genealogy. Virus Genes 40:320–328. https://doi.org/10.1007/s11262-010-0450-2.
13. Albariño CG, Bird BH, Chakrabarti AK, Dodd KA, Flint M, Bergeron E, White DM, Nichol ST. 2011. The major determinant of attenuation in mice of the candid1 vaccine for Argentine hemorrhagic fever is located in the g2 glycoprotein transmembrane domain. J Virol 85:10404–10408. https://doi.org/10.1128/JVI.00856-11.
14. Seregin AV, Yun NE, Miller M, Aronson J, Smith JK, Walker AG, Smith JN, Huang C, Manning JT, de la Torre JC, Paessler S. 2015. The glycoprotein precursor gene of Junin virus determines the virulence of the Romero strain and the attenuation of the Candid #1 strain in a representative animal model of Argentine hemorrhagic fever. J Virol 89:5949–5956. https://doi.org/10.1128/JVI.00104-15.
15. Radoshitzky SR, Abraham J, Spiropoulou CF, Kuhn JH, Nguyen D, Li W, Nagel J, Schmidt PJ, Nunberg JH, Andrews NC, Farzan M, Choe H. 2007. Transferrin receptor 1 is a cellular receptor for New World haemorrhagic fever arenaviruses. Nature 446:92–96. https://doi.org/10.1038/nature05539.
16. Di Simone C, Zandonatti MA, Buchmeier MJ. 1994. Acidic pH triggers

LCMV membrane fusion activity and conformational change in the glycoprotein spike. Virology 198:455–465. https://doi.org/10.1006/viro.1994.1057.
17. Eichler R, Lenz O, Strecker T, Garten W. 2003. Signal peptide of Lassa virus glycoprotein GP-C exhibits an unusual length. FEBS Lett 538:203–206. https://doi.org/10.1016/S0014-5793(03)00160-1.
18. York J, Romanowski V, Lu M, Nunberg JH. 2004. The signal peptide of the Junín arenavirus envelope glycoprotein is myristoylated and forms an essential subunit of the mature G1-G2 complex. J Virol 78:10783–10792. https://doi.org/10.1128/JVI.78.19.10783-10792.2004.
19. Agnihothram SS, York J, Trahey M, Nunberg JH. 2007. Bitopic membrane topology of the stable signal peptide in the tripartite Junín virus GP-C envelope glycoprotein complex. J Virol 81:4331–4337. https://doi.org/10.1128/JVI.02779-06.
20. York J, Nunberg JH. 2006. Role of the stable signal peptide of the Junín arenavirus envelope glycoprotein in pH-dependent membrane fusion. J Virol 80:7775–7780. https://doi.org/10.1128/JVI.00642-06.
21. York J, Nunberg JH. 2009. Intersubunit interactions modulate pH-induced activation of membrane fusion by the Junin virus envelope glycoprotein GPC. J Virol 83:4121–4126. https://doi.org/10.1128/JVI.02410-08.
22. Messina EL, York J, Nunberg JH. 2012. Dissection of the role of the stable signal peptide of the arenavirus envelope glycoprotein in membrane fusion. J Virol 86:6138–6145. https://doi.org/10.1128/JVI.07241-11.
23. Ghiringhelli PD, Rivera-Pomar RV, Lozano ME, Grau O, Romanowski V. 1991. Molecular organization of Junin virus S RNA: complete nucleotide sequence, relationship with other members of the Arenaviridae and unusual secondary structures. J Gen Virol 72:2129–2141. https://doi.org/10.1099/0022-1317-72-9-2129.
24. Albariño CG, Bergeron E, Erickson BR, Khristova ML, Rollin PE, Nichol ST. 2009. Efficient reverse genetics generation of infectious Junin viruses differing in glycoprotein processing. J Virol 83:5606–5614. https://doi.org/10.1128/JVI.00276-09.
25. Manning J, Seregin A, Yun N, Koma T, Huang C, Barral J, de la Torre J, Paessler S. 2017. Absence of an N-linked glycosylation motif in the glycoprotein of the live-attenuated Argentine hemorrhagic fever vaccine, Candid#1, results in its improper processing, and reduced surface expression. Front Cell Infect Microbiol 7:20. https://doi.org/10.3389/fcimb.2017.00020.
26. Droniou-Bonzom ME, Reignier T, Oldenburg JE, Cox AU, Exline CM, Rathbun JY, Cannon PM. 2011. Substitutions in the glycoprotein (GP) of the Candid#1 vaccine strain of Junin virus increase dependence on human transferrin receptor 1 for entry and destabilize the metastable conformation of GP. J Virol 85:13457–13462. https://doi.org/10.1128/JVI.05616-11.
27. Emonet SF, Seregin AV, Yun NE, Poussard AL, Walker AG, de la Torre JC, Paessler S. 2011. Rescue from cloned cDNAs and in vivo characterization of recombinant pathogenic Romero and live-attenuated Candid #1 strains of Junin virus, the causative agent of Argentine hemorrhagic fever disease. J Virol 85:1473–1483. https://doi.org/10.1128/JVI.02102-10.
28. York J, Nunberg JH. 2016. Myristoylation of the arenavirus envelope glycoprotein stable signal peptide is critical for membrane fusion but dispensable for virion morphogenesis. J Virol 90:8341–8350. https://doi.org/10.1128/JVI.01124-16.
29. Eichler R, Lenz O, Strecker T, Eickmann M, Klenk HD, Garten W. 2003. Identification of Lassa virus glycoprotein signal peptide as a trans-acting maturation factor. EMBO Rep 4:1084–1088. https://doi.org/10.1038/sj.embor.7400002.
30. Contigiani M, Medeot S, Diaz G. 1993. Heterogeneity and stability characteristics of Candid 1 attenuated strain of Junin virus. Acta Virol 37:41–46.
31. Grande-Perez A, Martin V, Moreno H, de la Torre JC. 2016. Arenavirus quasispecies and their biological implications. Curr Top Microbiol Immunol 392:231–276.
32. York J, Dai D, Amberg SA, Nunberg JH. 2008. pH-induced activation of arenavirus membrane fusion is antagonized by small-molecule inhibitors. J Virol 82:10932–10939. https://doi.org/10.1128/JVI.01140-08.
33. Shankar S, Whitby LR, Casquilho-Gray HE, York J, Boger DL, Nunberg JH. 2016. Small-molecule fusion inhibitors bind the pH-sensing SSP-GP2 subunit interface of the Lassa virus envelope glycoprotein. J Virol 90:6799–6807. https://doi.org/10.1128/JVI.00597-16.
34. Agnihothram SS, York J, Nunberg JH. 2006. Role of the stable signal peptide and cytoplasmic domain of G2 in regulating intracellular transport of the Junin virus envelope glycoprotein complex. J Virol 80:5189–5198. https://doi.org/10.1128/JVI.00208-06.
35. Hastie KM, Igonet S, Sullivan BM, Legrand P, Zandonatti MA, Robinson JE, Garry RF, Rey FA, Oldstone MB, Saphire EO. 2016. Crystal structure of the prefusion surface glycoprotein of the prototypic arenavirus LCMV. Nat Struct Mol Biol 23:513–521. https://doi.org/10.1038/nsmb.3210.
36. Hastie KM, Zandonatti MA, Kleinfelter LM, Heinrich ML, Rowland MM, Chandran K, Branco LM, Robinson JE, Garry RF, Saphire EO. 2017. Structural basis for antibody-mediated neutralization of Lassa virus. Science 356:923–928. https://doi.org/10.1126/science.aam7260.
37. Klewitz C, Klenk HD, ter Meulen J. 2007. Amino acids from both N-terminal hydrophobic regions of the Lassa virus envelope glycoprotein GP-2 are critical for pH-dependent membrane fusion and infectivity. J Gen Virol 88:2320–2328. https://doi.org/10.1099/vir.0.82950-0.
38. York J, Berry JD, Ströher U, Li Q, Feldmann H, Lu M, Trahey M, Nunberg JH. 2010. An antibody directed against the fusion peptide of Junin virus envelope glycoprotein GPC inhibits pH-induced membrane fusion. J Virol 84:6119–6129. https://doi.org/10.1128/JVI.02700-09.
39. Volpon L, Osborne MJ, Borden KL. 2008. NMR assignment of the arenaviral protein Z from Lassa fever virus. Biomol NMR Assign 2:81–84. https://doi.org/10.1007/s12104-008-9090-z.
40. Capul AA, de la Torre JC, Buchmeier MJ. 2011. Conserved residues in Lassa fever virus Z protein modulate viral infectivity at the level of the ribonucleoprotein. J Virol 85:3172–3178. https://doi.org/10.1128/JVI.02081-10.
41. Larson RA, Dai D, Hosack VT, Tan Y, Bolken TC, Hruby DE, Amberg SM. 2008. Identification of a broad-spectrum arenavirus entry inhibitor. J Virol 82:10768–10775. https://doi.org/10.1128/JVI.00941-08.
42. Jae LT, Brummelkamp TR. 2015. Emerging intracellular receptors for hemorrhagic fever viruses. Trends Microbiol 23:392–400. https://doi.org/10.1016/j.tim.2015.04.006.
43. Rojek JM, Kunz S. 2008. Cell entry by human pathogenic arenaviruses. Cell Microbiol 10:828–835. https://doi.org/10.1111/j.1462-5822.2007.01113.x.
44. Jae LT, Raaben M, Herbert AS, Kuehne AI, Wirchnianski AS, Soh TK, Stubbs SH, Janssen H, Damme M, Saftig P, Whelan SP, Dye JM, Brummelkamp TR. 2014. Virus entry. Lassa virus entry requires a trigger-induced receptor switch. Science 344:1506–1510.
45. Igonet S, Vaney MC, Vonhrein C, Bricogne G, Stura EA, Hengartner H, Eschli B, Rey FA. 2011. X-ray structure of the arenavirus glycoprotein GP2 in its postfusion hairpin conformation. Proc Natl Acad Sci U S A 108:19967–19972. https://doi.org/10.1073/pnas.1108910108.
46. Lee AM, Rojek JM, Spiropoulou CF, Gundersen AT, Jin W, Shaginian A, York J, Nunberg JH, Boger DL, Oldstone MBA, Kunz S. 2008. Unique small molecule entry inhibitors of hemorrhagic fever arenaviruses. J Biol Chem 283:18734–18742. https://doi.org/10.1074/jbc.M802089200.
47. York J, Nunberg JH. 2007. Distinct requirements for signal peptidase processing and function of the stable signal peptide (SSP) subunit in the Junin virus envelope glycoprotein. Virology 359:72–81. https://doi.org/10.1016/j.virol.2006.08.048.
48. Fuerst TR, Niles EG, Studier FW, Moss B. 1986. Eukaryotic transient-expression system based on recombinant vaccinia virus that synthesizes bacteriophage T7 RNA polymerase. Proc Natl Acad Sci U S A 83:8122–8126. https://doi.org/10.1073/pnas.83.21.8122.
49. Nussbaum O, Broder CC, Berger EA. 1994. Fusogenic mechanisms of enveloped–virus glycoproteins analyzed by a novel recombinant vaccinia virus-based assay quantitating cell fusion–dependent reporter gene activation. J Virol 68:5411–5422.
50. Baird NL, York J, Nunberg JH. 2012. Arenavirus infection induces discrete cytosolic structures for RNA replication. J Virol 86:11301–11310. https://doi.org/10.1128/JVI.01635-12.
51. Li H, Durbin R. 2009. Fast and accurate short read alignment with Burrows-Wheeler transform. Bioinformatics 25:1754–1760. https://doi.org/10.1093/bioinformatics/btp324.
52. Li H, Handsaker B, Wysoker A, Fennell T, Ruan J, Homer N, Marth G, Abecasis G, Durbin R. 2009. The Sequence Alignment/Map format and SAMtools. Bioinformatics 25:2078–2079. https://doi.org/10.1093/bioinformatics/btp352.
53. Robinson JT, Thorvaldsdottir H, Winckler W, Guttman M, Lander ES, Getz G, Mesirov JP. 2011. Integrative genomics viewer. Nat Biotechnol 29:24–26. https://doi.org/10.1038/nbt.1754.